Convolution approach for analysis of magnetic forces in electrical machines

R. Rothe, M. van der Giet and K. Hameyer
Institute of Electrical Machines, RWTH Aachen University, Aachen, Germany

Abstract

Purpose – The purpose of this paper is to present a method for analyzing higher magnetic force harmonics in electrical machines based on electromagnetic finite element simulation.

Design/methodology/approach – Sampling of air gap field solution data allows for a Fourier decomposition of magnetic forces and flux densities. A two-dimensional convolution gives insight into the spectral decomposition of forces responsible for acoustic noise, vibration and higher torque harmonics.

Findings – The proposed approach seems especially suitable for synchronous machine models. The influence of magnetic circuit design parameters that are difficult to calculate analytically on the harmonic air gap content can be analyzed and the spectral force decomposition illustrated by means of space vectors.

Originality/value – The approach is generalized to the convolution and analysis of arbitrarily sampled two-dimensional data in this paper.

Keywords Electric machines, Magnetic measurement, Force measurement, Harmonics, Finite element analysis, Vibration

Paper type Research paper

I. Introduction

Higher torque harmonics and magnetically excited noise are parasitic effects in electrical machines. They are due to the harmonic forces in the air gap of the machine. Acting on the permeable material of stator and rotor, not only a constant torque but also additional torque harmonics are generated, as well as radial forces that excite stator vibrations. These electromagnetic forces can be calculated from the air gap field.

Electromagnetic finite element method (FEM) analyses are used to calculate torques, but also allow for a consideration of local values, such as the magnetic flux density distribution in the air gap. This paper proposes to sample the air gap field solution data of two-dimensional FEM simulations in time and space domain in order to perform a Fourier decomposition and a subsequent two-dimensional periodic convolution of air gap field data. This leads to a geometric addition of partial force components that can be visualized by a space vector diagram. The method has been applied to the radial component of the air gap field for noise analysis purposes (van der Giet *et al.*, 2008), and it is generalized in this paper to the convolution of arbitrary sampled two-dimensional data.

In the following method and its implementation are described. First, some basic Fourier theory is introduced. For an analysis of torque harmonics and noise exciting radial forces, the method is applied to a sinusoidally fed permanent magnet-excited synchronous machine (PMSM) and induction machine (IM) model.

The authors would like to thank contributors to the success of the EMF 2009 Symposium.

COMPEL: The International Journal for Computation and Mathematics in Electrical and Electronic Engineering
Vol. 29 No. 6, 2010
pp. 1542-1551

0332-1649
DOI 10.1108/03321641011078616

II. Convolution approach

A. Two-dimensional Fourier decomposition and periodic convolution

Since the air gap field and the forces are periodic in time and space, they can be represented by a Fourier series. Let p: $\mathbb{R} \times \mathbb{R} \rightarrow \mathbb{R}$ be continuously differentiable. One has:

$$p(\tilde{x}, t) = \sum_{n=-\infty}^{\infty} \sum_{m=-\infty}^{\infty} P_{n,m} e^{j(m\Delta r\tilde{x} + n\Delta\omega t)}, \tag{1}$$

$\Delta\omega = 2\pi/T$, $\Delta r = 2\pi/U$ with T, $U > 0$ the periods in time and space. The complex Fourier coefficients are determined by:

$$P_{n,m} = \frac{1}{U}\,\frac{1}{T} \int_0^U \int_0^T p(\tilde{x}, t) e^{-j(m\Delta r\tilde{x} + n\Delta\omega t)} dt d\tilde{x}. \tag{2}$$

For a Fourier decomposition (Figure 1), many tools process sampled data $y_{n,m}$ by using the discrete Fourier transformation (DFT). The two-dimensional DFT is defined by:

$$\mathcal{F}(y_{n,m}) = Y_{n,m} = \sum_{l=0}^{N-1} \sum_{k=0}^{M-1} y_{l,k} e^{-2\pi j((nl/N) + (mk/M))}, \tag{3}$$

where $n = 0 \ldots (N-1)$, $m = 0 \ldots (M-1)$. In order to approximate the Fourier series coefficients with Fourier transformation coefficients, a full space-time period U and T is sampled with M and N equidistant steps. The double integral of equation (2) can be approximated by sums, and after some rearrangements the coefficient approximation results to:

$$P_{n,m} \approx \frac{Y_{n,m}}{MN}. \tag{4}$$

Using Maxwell's stress tensor, tangential force calculation is obtained by the multiplication of normal and tangential air gap field components. The multiplication of values of two sampled data sets $z_{l,k}$ and $z'_{l,k}$ becomes in the frequency-mode domain a periodic convolution:

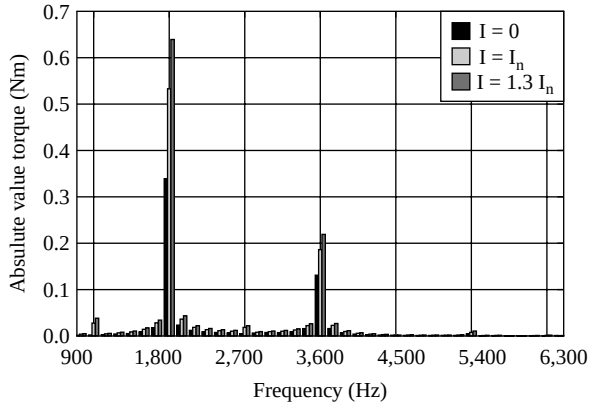

Figure 1.
One-dimensional Fourier decomposition of the output torque (van Riesen *et al.*, 2004) of the PMSM model, $n = 4{,}500$ rpm, higher harmonics

$$y_{n,m} = z_{n,m} \cdot z'_{n,m} \Leftrightarrow Y_{n,m} = Z_{n,m} * Z'_{n,m}, \tag{5}$$

with:

$$Z_{n,m} * Z'_{n,m} = \frac{1}{MN} \sum_{l=0}^{N-1} \sum_{k=0}^{M-1} Z_{l,k} \cdot Z'_{n-l,m-k} \equiv \sum_{l,k} Q_{n,m,l,k} \cdot MN. \tag{6}$$

B. Sampling of FEM solution data

In practice, the sampled data are stored into arrays *y, z* and the two-dimensional DFT is performed by a computer routine. The resulting matrices *Y, Z* contain the complex Fourier transformation coefficients. Provided that a full space-time period is sampled, the row number n of Y or Z corresponds to the temporal ordinal number and the column number m corresponds to the spacial ordinal number, which is usually called mode or number of pole pair. Each matrix entry $Y_{n,m}$ or $Z_{n,m}$ can be interpreted as a one-dimensional sinusoidal wave. Assuming that matrix z contains sampled data of the radial component of the magnetic flux density in the air gap, a single sinusoidal wave can be expressed by:

$$b^r(x,t) = 2\left|\frac{Z_{n,m}}{MN}\right| \frac{\mathrm{Vs}}{\mathrm{m}^2} \cdot \cos\left(mx + n\Delta\omega t + \arg\left(\frac{Z_{n,m}}{MN}\right)\right). \tag{7}$$

This notation is common in analytical considerations of higher air gap field harmonics, (Jordan, 1950; Gieras *et al.*, 2006). Note that the same harmonic wave is obtained by inversion of the argument of the cosine function, and hence an inversion of the sign of the ordinal numbers. This indicates the symmetry of the DFT transformed matrix:

$$Z_{n,m} = Z^*_{-n,-m}. \tag{8}$$

C. Calculation of magnetic forces

Based on the Maxwell stress tensor, the magnetic force vector can be expressed in polar coordinates by:

$$\begin{aligned} \boldsymbol{p} &= \boldsymbol{p}^t + \boldsymbol{p}^r \\ &= b^r h^t \boldsymbol{e}^t + \frac{1}{2\mu_0}[(b^r)^2 - (b^t)^2]\boldsymbol{e}^r, \end{aligned} \tag{9}$$

where $\boldsymbol{e}^t, \boldsymbol{e}^r$ are polar unit vectors. Discrete data of the radial and tangential air gap field solution $b^r_{n,m}, b^t_{n,m}$ can be obtained by data sampling. Since the DFT is a linear map, a Fourier transformation and a division by $(MN)^2$ according to approximation (4) results to:

$$\frac{\mathcal{F}(\boldsymbol{p}_{n,m})}{(MN)^2} = B^r_{n,m} * H^t_{n,m} \boldsymbol{e}^t + \frac{1}{2\mu_0}\left[B^r_{n,m} * B^r_{n,m} - B^t_{n,m} * B^t_{n,m}\right]\boldsymbol{e}^r. \tag{10}$$

The tangential component of the air gap field is very small when compared to the radial one. Therefore, equation (10) is frequently approximated by the simplified Maxwell stress tensor. Then the Fourier series coefficients of the force densities result to:

$$\boldsymbol{P}_{n,m} = \frac{\mathcal{F}(P_{n,m})}{MN} = \underbrace{MN \cdot B^r_{n,m} * H^t_{n,m}}_{=P^t_{n,m}} \boldsymbol{e}^t + \underbrace{\frac{MN}{2\mu_0} \cdot B^r_{n,m} * B^r_{n,m}}_{=P^r_{n,m}} \boldsymbol{e}^r. \tag{11}$$

Two convolution products remain. The tangential forces generate the torque and the radial forces are the main cause for vibration and noise radiation of electrical machines. Normally, the magnetic force density coefficients $P^r_{n,m}$ and $P^t_{n,m}$ are obtained by first multiplying the air gap fields and transferring to the space-time domain. Alternatively, using the convolution allows for a consideration of the summands $Q_{n,m,l,k}$ in equation (6) as explored in the next section.

D. Visualization with a space vector diagram

Equation (6) shows that the matrix entries of Z are combined by pairs and add up to the total Fourier transformation component $Y_{n,m}$. The geometric addition can be supported by an illustration in the complex plane called space vector diagram, Figure 2. Implemented to a computer routine, partial force Fourier series summands $Q_{n,m,l,k}$ and the associated air gap field pair. Fourier components are stored for a subsequent visualization.

In the following, the four pole PMSM is considered, Figure 3. A two-dimensional FE simulation reveals that besides the constant torque component, undesired torque harmonics emerge, especially at $f = 1{,}800$ Hz, Figure 1. The proposed convolution approach is applied. The radial magnetic flux density component b^r and the tangential magnetic strength component h^t are sampled. The convolution routine transfers the sampled data into the frequency-mode domain and generates the space vector diagram of the corresponding tangential Fourier series component $P^t_{24,0}$, Figure 2. The vector chain represents the geometric addition of partial force vectors:

$$Q_{l,k} = B^r_{l,k} \cdot H^t_{n-l,m-k}. \tag{12}$$

The involved air gap field harmonic combination pairs are listed in Table I. The ordinal numbers l, k, $n - l$, $m - k$ and the angle have to be added according to equations (6) and (12). Obviously, only a small number of pairs contribute significantly to the total Fourier series force component $P^t_{24,0}$. The vectors $Q_{l,k}$ are arranged

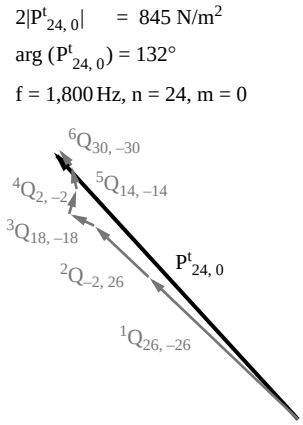

Figure 2.
Space vector diagram, $I = I_n$

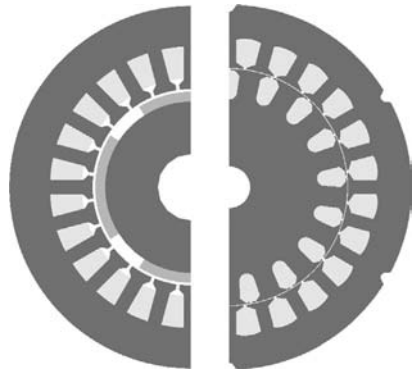

(a) PMSM **(b)** IM

Figure 3.
Scaled cross sections of example machines

Vec	l	k	$2\lvert B^r\rvert$ (Vs/m^2)	arg (B^r)[°]	f (Hz)
1	26	−26	0.043677	0.0	1,950
2	−2	26	0.027674	46.5	−150
3	18	−18	0.081638	180.0	1,350
4	2	−2	1.053000	6.6	150
5	14	−14	0.141511	0.3	1,050
6	30	−30	0.048354	180.0	2,250
Vec	$n-l$	$m-k$	$2\lvert H^t\rvert$ (A/m)	arg (H^t)[°]	f (Hz)
1	−2	26	21,793	136.4	−150
2	26	−26	12,481	90.1	1,950
3	6	18	1,559	−25.12	450
4	22	2	113	66.5	1,650
5	10	14	795	102.3	750
6	−6	30	2,028	51.4	−450

Table I.
Air gap field Fourier series components for $I = I_n$

according to their magnitude. Only the first six partial force vectors are depicted. Therefore, a small gap between the vector chain and the total force vector remains.

III. Application to machine models

A. PMSM model

A rule of thumb for predicting the frequency of the main parasitic torque harmonic is the least common multiple of the number of poles and the number of stator slots, LCM($2p$, N_s) (Herranz Gracia, 2009). This harmonic is usually called cogging torque or torque ripple. The considered PMSM has 24 slots, $p = 2$ and the LCM is 24, Table II. Since the speed of the machine is $n_n = 4{,}500$ rpm, the expected parasitic torque frequency is $f = 1{,}800$ Hz. The Fourier decomposition of the torque output of the used FE software (van Riesen *et al.*, 2004) meets this prediction, Figure 1.

The cogging component is due to the interaction of the magnetomotive force of the magnets Θ_M and the DC and fundamental component of the stator permeance function Λ, shown in Figure 4, where m is the defined spacial ordinal number, $g_1, g_2, g_3 \in \mathbb{N}$ and $f_1 = 150$ Hz is the frequency of the fundamental air gap field component (Herranz Gracia, 2009; Gieras *et al.*, 2006). The analytically derived and involved air gap field

Machine data	PMSM	IM
Rated power P_n	4 kW	30 kW
Rated speed n_n	4,500 rpm	3,000 rpm
Rated voltage V_n	230 V	400 V
Rated current I_n	11.2 A	55.6 A
Power factor $cos\varphi_n$	–	0.875
Number of pole pairs p	2	2
Number of stator slots N_S	24	24
PM material	NeFeBo	–
Outer stator diameter D_o	110 mm	232 mm
Air gap sampling radius	29.29 mm	85.75 mm
Mechanical air gap δ	0.8 mm	0.5 mm
Active length l_{Fe}	120 mm	127 mm

Table II.
Machine data

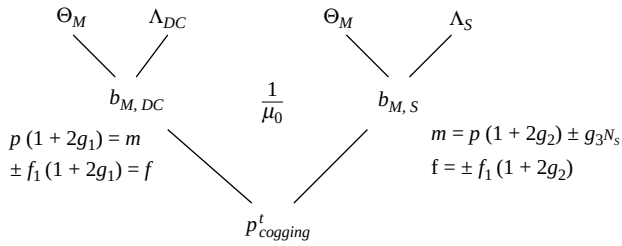

Figure 4.
Excitation of tangential cogging forces

components $b_{M,DC}$ and $b_{M,S}$ as well as the fundamental air gap field component b_1 can be assigned to the decomposition output of the convolution routine by means of their analytically known ordinal numbers. Table III lists the involved air gap field convolution pairs of two other simulated operating points $I = 0$ and $I = 1.3 \cdot I_n$ and Figure 5 shows the geometric addition. The angle between stator field and rotor position remains unchanged.

Using a sampling procedure and a DFT, a single sinusoidal wave is always described by two Fourier coefficients together that differ only in the sign of their angle and ordinal numbers according to equation (8). In Table III(b) the fundamental air gap field component b_1 appears two times with inverse values. In fact, both expressions describe the same wave. On the contrary to this, the known analytical derivations employ one expression for one sinusoidal wave by allowing only positive frequencies or positive modes (Gieras *et al.*, 2006).

Compared to the no load case (b), the parasitic force $P^t_{24,0}$ in (a) is increased in magnitude and the angles are distorted, Figure 5. This can be attributed to the increase of the tangential magnetic strength components H^t generated by the stator currents. Nearly, no new partial force vectors $Q_{l,k}$ do appear.

B. IM model

The introduced PMSM model offers an easy handling by sampling one rotor revolution or only one pole pitch revolution. The air gap field of the IM revolves asynchronously compared to the rotor. Thus, several rotor revolutions have to be simulated in order to allow for a sampling of a complete time period. If a transient simulation is chosen,

(*a*)	*l*	*k*	2 $\lvert B^r\rvert$ (Vs/m^2)	arg(B^r)[°]	*f* (Hz)	
1	26	−26	0.043481	0.1	1,950.0	$b'_{M,DC}$
2	−2	26	0.032443	53.1	−150.0	$b'_{M,S}$
3	18	−18	0.081647	−179.9	1,350.0	$b'_{M,DC}$
4	14	−14	0.141253	0.4	1,050.0	$b'_{M,DC}$
5	2	−2	1.055650	8.6	150.0	b_1
6	30	−30	0.048323	180.0	2,250.0	$b'_{M,DC}$
(*a*)	$n-l$	$m-k$	2$\lvert H^t\rvert$ (A/m)	arg(H^t)[°]	*f* (Hz)	
1	−2	26	2,5561	143.0	−150.0	$B'_{M,S}$
2	26	−26	1,2416	90.3	1950.0	$b'_{M,DC}$
3	6	18	1,938	−12.5	450.0	$b'_{M,S}$
4	10	14	1,099	105.0	750.0	$b'_{M,S}$
5	22	2	140	67.9	1650.0	$b'_{M,S}$
6	−6	30	2,506	−45.7	−450.0	$b'_{M,DC}$
(*b*)	*l*	*k*	2$\lvert B^r\rvert$ (Vs/m^2)	arg(B^r)[°]	*f* (Hz)	
1	26	−26	0.043507	−0.2	1,950.0	$b_{M,DC}$
2	−2	26	0.018125	−0.0	−150.0	$b_{M,S}$
3	18	−18	0.081554	180.0	1,350.0	$b_{M,DC}$
4	−2	2	1.051050	0.0	−150.0	b_1
5	2	−2	1.051050	−0.0	150.0	b_1
6	30	−30	0.048426	179.9	2,250.0	$b_{M,DC}$
7	14	−14	0.141744	−0.0	1,050.0	$b_{M,DC}$
8	34	−34	0.023964	0.0	2,550.0	$b_{M,DC}$
(*b*)	$n-l$	$m-k$	2$\lvert H^t\rvert$ (A/m)	arg(H^t)[°]	*f* (Hz)	
1	−2	26	14,322	90.0	−150.0	$b_{M,S}$
2	26	−26	12,388	89.8	1,950.0	$b_{M,DC}$
3	6	18	991	−90.0	450.0	$b_{M,S}$
4	26	−2	75	−90.6	1,950.0	
5	22	2	59	90.3	1,650.0	
6	−6	30	1,293	−90.1	−450.0	$b_{M,S}$
7	10	14	388	90.0	750.0	$b_{M,DC}$
8	−10	34	2,233	−90.0	−750.0	$b_{M,DC}$

Table III.
Air gap field components for (a) $I = 1.3 \cdot I_n$ and (b) $I = 0$

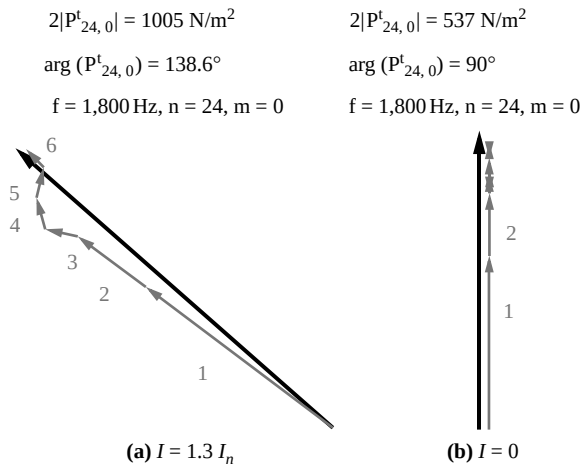

Figure 5.
Space vector diagrams for $P^t_{24,0}$

additional time steps are necessary to magnetize the rotor until steady state behavior is reached. The considered IM has been simulated for slip $s = 0.008$ and afterwards 62 rotor revolutions have been sampled.

The radial component of the magnetic forces is the main cause for electromagnetically excited vibration and noise radiation. However, the intensity is strongly determined by the distribution of the natural frequencies of the mechanical housing. Also the modes $m = -6 \ldots 6$ with high mechanical amplifications are of special interest in contrast to the torque, that is solely generated by forces with $m = 0$. The maximum air gap field components and their identification and the maximum forces are listed in Table IV. The natural frequencies of the considered IM housing are unknown, therefore the radial example force component is $P^r_{2608,3}$ is singled out for analysis (Figure 6 and Table V). The partial force components are analogous to equation (12):

$$Q_{l,k} = \frac{1}{2\mu_0} B^r_{l,k} \cdot B^r_{n-l,m-k}. \tag{13}$$

$2\lvert B^r\rvert$ (Vs/m^2)	$\arg(B^r)$[°]	n	m	f (Hz)	
0.931856	−47.3	250	−2	100.806	fundam.
0.194274	−15.2	250	22	100.806	stat. slot.
0.176265	−102.3	2,358	−19	950.806	rot. slot.
0.166318	20.7	1,858	−15	749.193	rot. slot.
0.106786	−161.8	250	−26	100.806	stat. slot.
0.104127	169.9	250	46	100.806	stat. slot.
0.090524	25.4	750	−6	302.419	saturation
$2\lvert P^r\rvert$ (N/m^2)	$\arg(P^r)$ [°]	n	m	f (Hz)	
423,884	0.0	0	0	0.0	–
139,173	−97.5	500	−4	201.612	–
24,806	−168.7	2,608	3	1051.612	–
11,040	39.8	3,092	1	1246.774	–
10,510	63.2	1,000	4	403.226	–
7,924	−35.0	608	−5	245.161	–
5,093	136.7	2,108	−5	850.000	–
4,510	68.5	500	2	201.612	–

Table IV.
Maximum air gap field and magnetic force components ($m = -6 \ldots 6$), $n \geq 0$

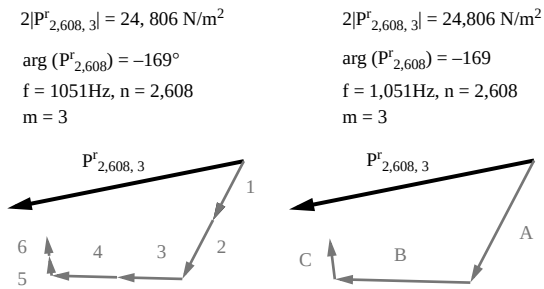

(a) Calculated partial vectors **(b)** Combined partial vectors

Sources: This paper approach; van der Giet *et al.*' (2008) paper approach

Figure 6.
Space vector diagrams for $P^r_{2608,3}$

Vec.	l	k	$2\lvert B^r\rvert$ (Vs/m^2)	arg(B^r) [°]	f (Hz)
1	250	22	0.194274	−15.2	100.806
2	2,358	−19	0.176265	−102.3	950.806
3	250	−2	0.931856	−47.3	100.806
4	2,358	5	0.036160	−134.2	950.806
5	1,858	−15	0.166318	20.7	749.194
6	750	18	0.061925	76.4	302.419
Vec.	$n-l$	$m-k$	$2\lvert B^r\rvert$ (Vs/m^2)	arg(B^r) [°]	f (Hz)
1	2,358	−19	0.176265	−102.3	950.806
2	250	22	0.194274	−15.2	100.806
3	2,358	5	0.036160	−134.2	950.806
4	250	−2	0.931856	−47.3	100.806
5	750	18	0.061925	76.4	302.419
6	1,858	−15	0.166318	20.7	749.194

Table V.
Air gap field components for Figure 6

IV. Conclusions

The proposed method delivers a deeper insight into the generation of parasitic magnetic forces in rotating electrical machines and may provide additional help for understanding and calculation of higher harmonics beside the analytical approaches. The influence of special design decisions, such as additional holes or notches, that are difficult to calculate analytically, or factors, such as excentricities or certain current shapes, can be analyzed by this way.

Since the output solution of any electromagnetic FEM software is the magnetic vector potential and so the magnetic flux density, an analysis of permeance functions or mmf distributions is not possible. The geometric addition of several air gap field components, excited from different causes, can only be indirectly detected, for instance, by two comparative simulation analyses.

The calculated torque of FEM software is strongly dependent on the mesh refinement in the air gap (Herranz Gracia, 2009). This should also be valid for higher air gap field harmonics. Further investigations concerning the influence of the air gap element size and the sample density on the calculated local magnetic forces are to be undertaken. Also a consideration of the neglected tangential air gap fields for the calculation of radial forces is to be taken into account.

The effort and costs for an analysis of the harmonic content of an IM model is considerable. Additionally, since a complete time period must be sampled, only discrete operating points are possible. Therefore, the proposed analysis seems especially suitable for synchronous machine models.

References

Gieras, J.F., Wang, C. and Cho Lai, J. (2006), *Noise of Polyphase Electric Motors*, CRC Press, Boca Raton, FL.

Herranz Gracia, M. (2009), *Methoden zum Entwurf von robusten Stellantrieben unter Berücksichtigung fertigungsbedingter Abweichungen*, Shaker Verlag, Institute of Electrical Machines, RWTH Aachen, Aachen.

Jordan, H. (1950), *Geräuscharme Elektromotoren*, W. Girardet, Essen, November.

van der Giet, M., Rothe, R., Herranz Gracia, M. and Hameyer, K. (2008), "Analysis of noise exciting magnetic force waves by means of numerical simulation and a space vector definition", *18th International Conference on Electrical Machines, ICEM 2008 Vilamoura, September*, pp. 1-6.

van Riesen, D., Monzel, C., Kaehler, C., Schlensok, C. and Henneberger, G. (2004), "iMOOSE – an open-source environment for finite-element calculations", *IEEE Transactions on Magnetics*, Vol. 40 No. 2, pp. 1390-3.

About the authors

R. Rothe received his Dipl-Ing degree in Electrical Engineering from the Faculty of Electrical Engineering and Information Technology at the RWTH Aachen University. Since 2007, he has worked as a researcher at the Institute of Electrical Machines (IEM) at the RWTH Aachen University. He is currently working towards his PhD degree and his research interests are the numerical field simulation of electro-magnetic devices. R. Rothe is the corresponding author and can be contacted at: Richard.Rothe@iem.rwth-aachen.de

M. van der Giet received his Dipl-Ing degree in Electrical Engineering in 2004 as Engineer from the Faculty of Electrical Engineering and Information Technology at the RWTH Aachen University. Since 2004, he has worked as a researcher at the IEM at the RWTH Aachen University and is currently Chief Engineer. He is working towards his PhD degree in the area of noise and vibration of electrical machines.

K. Hameyer received the Dipl-Ing degree in Electrical Engineering from the University of Hannover, Germany. He received the PhD degree from University of Technology, Berlin, Germany. After his university studies, he worked with the Robert Bosch GmbH in Stuttgart, Germany, as a Design Engineer for permanent magnet servo motors and board net components. In 1988, he became a member of the staff at the University of Technology, Berlin, Germany. Until February 2004, K. Hameyer was a full Professor for Numerical Field Computations and Electrical Machines with the KU Leuven in Belgium. Currently, K. Hameyer is the Head of the IEM and holder of the Chair Electromagnetic Energy Conversion at the RWTH Aachen University in Germany. His research interests are numerical field computation, the design of electrical machines, in particular permanent magnet-excited machines, IMs and numerical optimization strategies.